



**HAL**  
open science

# Dyke propagation and sill formation in a compressive tectonic environment

T. Menand, K. Daniels, P. Benghiat

► **To cite this version:**

T. Menand, K. Daniels, P. Benghiat. Dyke propagation and sill formation in a compressive tectonic environment. *Journal of Geophysical Research*, 2010, 115 (B8), 10.1029/2009JB006791 . hal-01892431

**HAL Id: hal-01892431**

**<https://uca.hal.science/hal-01892431>**

Submitted on 24 Nov 2020

**HAL** is a multi-disciplinary open access archive for the deposit and dissemination of scientific research documents, whether they are published or not. The documents may come from teaching and research institutions in France or abroad, or from public or private research centers.

L'archive ouverte pluridisciplinaire **HAL**, est destinée au dépôt et à la diffusion de documents scientifiques de niveau recherche, publiés ou non, émanant des établissements d'enseignement et de recherche français ou étrangers, des laboratoires publics ou privés.



Distributed under a Creative Commons Attribution 4.0 International License

## Dyke propagation and sill formation in a compressive tectonic environment

T. Menand,<sup>1</sup> K. A. Daniels,<sup>1</sup> and P. Benghiat<sup>1,2</sup>

Received 16 July 2009; revised 19 March 2010; accepted 25 March 2010; published 6 August 2010.

[1] Sills could potentially form as a result of dykes modifying their trajectory in response to remote tectonic compression. Here, we use analogue experiments to investigate how a buoyant vertical dyke adjusts its trajectory to a compressive remote stress to form a sill, and over which vertical distance this sill formation does occur. Our investigation is restricted to an intrusion propagating through a homogeneous solid, which enables us to identify the characteristic length-scale over which a dyke responds to remote stress compression, independently of the presence of crustal layers. The experiments involve the injection of air in a gelatine solid that experiences lateral deviatoric compression. The response of the buoyant air crack to the compressive stress is not instantaneous but operates over some distance. An important observation is that some cracks reach the surface despite the compressive environment. Dyke-to-sill rotation occurs only for large compressive stress or small effective buoyancy. Dimensional analysis shows that the length-scale over which this rotation takes place increases exponentially with the ratio of crack effective buoyancy to horizontal compressive stress. Up-scaled to geological conditions, our analysis indicates that a dyke-to-sill transition in response to tectonic compression in homogeneous rocks cannot occur over less than two hundred meters and would need several kilometers in most cases. This is typically greater than the average thickness of lithological units, which supports the idea that crustal heterogeneities play an important role in determining the fate of dykes and in controlling where sills could form.

**Citation:** Menand, T., K. A. Daniels, and P. Benghiat (2010), Dyke propagation and sill formation in a compressive tectonic environment, *J. Geophys. Res.*, 115, B08201, doi:10.1029/2009JB006791.

### 1. Introduction

[2] The transport of magma from its source regions up to the Earth's surface occurs essentially via vertical or sub-vertical dykes, which ultimately feed volcanoes. However, not all dykes lead to eruptions. In fact, the vast majority of dykes stall en route and remain trapped in the crust. Ratios of intrusive to extrusive magma volumes have been estimated to be of the order of 10: 1 [Crisp, 1984; Shaw, 1985] whilst Gudmundsson *et al.* [1999] have calculated that the actual proportion of dykes reaching the surface in Iceland and Tenerife, Canary Islands, is only a few %. In many cases, those dykes which did not make it to the surface are associated with the formation or feeding of sub-horizontal sills [e.g., Gudmundsson *et al.*, 1999; Burchardt, 2008]. Sills could therefore be envisaged as either arresting the advance of dykes or, conversely, forming as a result of dykes being prevented from propagating further.

[3] There is a renewed interest in the formation of sills because they are increasingly recognized as being the building blocks of larger magma chambers and their frozen equivalent that are laccoliths, plutons and other larger batholiths [Gudmundsson, 1990; Menand, 2008]. Indeed, there is mounting geological, geophysical and geochronological evidence that plutons grow by the amalgamation of individual intrusive igneous sheets [Bedard *et al.*, 1988; John, 1988; Hutton, 1992; John and Blundy, 1993; Vignerresse and Bouchez, 1997; Wiebe and Collins, 1998; Coleman *et al.*, 2004; Glazner *et al.*, 2004; Horsman *et al.*, 2005, 2008; Morgan *et al.*, 2005, 2008; Belcher and Kisters, 2006; de Saint-Blanquat *et al.*, 2006; Pasquarè and Tibaldi, 2007]. Consequently, sills are also being recognized as potential sites of magma differentiation [Annen and Sparks, 2002; Annen *et al.*, 2006; Michaut and Jaupart, 2006].

[4] Sills form when their feeder dyke stops propagating mainly vertically and instead intrude concordantly along a lithological plane of weakness. However, the vast majority of magmatic intrusions are discordant, and so the mere presence of lithological discontinuities or planes of weakness is not a sufficient condition for the formation of sills. This observation is also corroborated by analogue experiments [Kavanagh *et al.*, 2006].

<sup>1</sup>Centre for Environmental and Geophysical Flows, Department of Earth Sciences, University of Bristol, Bristol, UK.

<sup>2</sup>Now at Atlas Iron Limited, West Perth, Western Australia, Australia.

[5] One of the early model for sill formation proposed that sills tend to form when dykes become neutrally buoyant and lose their vertical driving force. Sills were therefore thought to form preferentially at levels of neutral buoyancy [Gilbert, 1877; Corry, 1988], that is at stratigraphic horizons where magma density equals that of the host rocks. However, this is contradicted by field and seismic data, which show many sills intruding successively different stratigraphic levels, likely characterized by different density [Johnson and Pollard, 1973; Cartwright and Hansen, 2006; Thomson, 2007]. This suggests that levels of neutral buoyancy do not provide a complete explanation for the mechanism and level of sill emplacement. In fact, as illustrated by the laboratory experiments of Lister and Kerr [1991], magma accumulation at levels of neutral buoyancy is more likely to involve lateral dyke propagation rather than sill formation because the latter case requires an additional rotation of the intrusion or the presence of a lithological plane of weakness that could be intruded. If a plane of weakness is present, levels of neutral buoyancy could assist sill formation, but Taisne and Jaupart [2009] showed that sill intrusion would still require very specific conditions with low-density stratigraphic layers that are at least 700-meter thick, and 2-kilometer thick on average. Other mechanisms that have been proposed for the formation of sills include the presence of layered rocks with rigidity contrast [Fridleifsson, 1977; Hyndman and Alt, 1987; Gudmundsson and Brenner, 2001; Holness and Humphreys, 2003; Rivalta et al., 2005; Kavanagh et al., 2006; Burchardt, 2008], rheology contrast between adjacent layers of elastic and ductile rocks [Mudge, 1968; Fridleifsson, 1977; Antonellini and Cambray, 1992; Watanabe et al., 1999], as well as the presence of weak layer contacts [e.g., Gudmundsson, 2003].

[6] Additionally, it has been observed that magmatic intrusions tend to orient themselves perpendicular to the least compressive stress. As a result they modify their propagation trajectories in response to spatial changes in, or rotation of, the surrounding stresses [Odé, 1957; Muller and Pollard, 1977; Dahm, 2000; Mériaux and Lister, 2002]. Therefore, an initially vertical dyke would be expected to turn into a horizontal sill if it were to become subjected to a horizontal compressive stress field where the least compressive stress is vertical [e.g., Gretener, 1969; Gudmundsson and Phillip, 2006]. However, theoretical studies have shown that the dynamics and direction of propagation of dykes depend on their buoyancy as well as the external deviatoric stress field including the stresses induced by the dykes themselves at their tip [e.g., Lister and Kerr, 1991; Dahm, 2000; Mériaux and Lister, 2002]. Also, the difference in density between rocks and magma is not the only source of buoyancy for dykes; vertical gradients of the normal external deviatoric stress contribute also to the effective buoyancy of the intrusions [Takada, 1989]. Therefore, whether propagating buoyant dykes could reach the Earth's surface or instead stall in the crust and lead to magma accumulation depends on the relative importance of their effective buoyancy and the ambient deviatoric stress [Watanabe et al., 1999; Dahm, 2000; Pinel and Jaupart, 2000, 2004]. The numerical work of Dahm [2000] and analogue experiments of Watanabe et al. [2002], for instance, show that dykes can stop their propagation and form sills, despite being buoyant, if they

experience relatively large stress gradients. Conversely, dykes could reach the surface even when experiencing a compressive stress field provided their effective buoyancy is large enough. As an example, Kühn and Dahm [2004, 2008] adapted and applied the model of Dahm [2000] to dyke propagation at mid-ocean ridges and showed how the relative strength of magma pressure and gradient of deviatoric stress could focus dykes as sheeted-dyke complex or instead lead to the formation of sill-like magma chambers.

[7] One key question that remains unanswered, however, is the length-scale over which a dyke-to-sill rotation occurs since this will determine whether a dyke can reach the surface or stalls as a sill instead. Both crustal heterogeneities and adequate stress field can lead to sill formation, but they involve separate length-scales.

[8] Gradients in or rotation of a stress field could be induced by various mechanisms and could thus occur over different length-scales. These mechanisms can, however, be sorted into two broad categories. A modification in stress field could occur because of remote, i.e. non localized, change or rotation. Magma initially originates from the mantle and propagates toward the surface through dykes, so the minimum compressive stress is likely to be horizontal in the lower crust. Yet crustal compressive and horizontal stress fields with a vertical minimum compressive stress, which would thus favor sill formation, do also exist. Stress rotation can also operate at the length-scale of a volcanic edifice, either in response to magma intrusion within the edifice [Roman et al., 2004, 2006] or as an effect of the load of the edifice itself [Watanabe et al., 2002; Pinel and Jaupart, 2004].

[9] The second type of mechanism that could induce stress rotation is more localized, and involves the presence of heterogeneous rock layers. For instance, a rheology contrast between a ductile rock layer and an adjacent elastic and brittle strata underneath might stop feeder dykes and promote sill formation into the ductile layer because the ductile zone would, at least partially, relax the pre-existing deviatoric stress favorable to dyke injection in the elastic layer [Parsons et al., 1992; Watanabe et al., 1999]. Alternatively, stress redistribution could also occur in layered elastic rocks with different mechanical properties. Adequate contrasts in Young's modulus and toughness between adjacent layers would lead to heterogeneous stress distribution with some layers concentrating horizontally compressive stress more than others [Gretener, 1969; Gudmundsson, 1986; Gudmundsson and Phillip, 2006]. Previously emplaced intrusions would also modify the ambient stress field. Such intrusion-induced stress anisotropy would affect the crust over distances proportional to the intrusion thickness [Westergaard, 1939], until it is relaxed by the crust.

[10] The key difference between these two broadly defined mechanisms for stress rotation is the presence, or absence, of crustal heterogeneous layered rocks; in one case stress anisotropy is induced by the presence of crustal heterogeneities (strata of different properties or previous intrusions), whereas in the other case stress rotation occurs remotely and whether heterogeneous rock strata are present or not. Here, we investigate (1) how a buoyant vertical dyke responds and adjusts its trajectory to a compressive remote stress to form a sill, and (2) over which vertical distance this sill

formation occurs. We restrict our investigation to the case of an intrusion propagating through a homogeneous elastic solid. This does not mean that crustal heterogeneities are considered unimportant for the growth and orientation of intrusions, or that our analysis only applies to homogeneous crustal regions. Rather, considering the case of a homogeneous crust enables us to identify the characteristic length-scale over which a dyke would respond to a remote stress rotation, independently of the potential presence of crustal layers and their properties. This will in turn enable us to quantify if and under which conditions crustal heterogeneities need to be taken into account when dealing with dyke propagation under anisotropic stress conditions. For the same reason, we limit ourselves to the case of a single intrusion, and do not investigate the effect previously formed sills could have on the propagation of subsequent intrusions. Although the state of stress in the Earth's crust can be complex, we also simplified our analysis to a uniform compressive deviatoric stress. Indeed, tectonic stresses have been shown to play an important role on the propagation of dykes only when their variations occur over the length scale of the dykes [Lister and Kerr, 1991; Dahm, 2000], and vertical stress gradients can be incorporated into the effective buoyancy force that drives the intrusion [Takada, 1989; Lister and Kerr, 1991]. Finally, we neglect any potential interaction between the intrusion and the free surface, which is a reasonable assumption provided the intrusion depth is greater than half the height of the intrusion [Rivalta and Dahm, 2006]. In section 2 we describe laboratory analogue experiments investigating the propagation of a buoyant crack in a compressive environment, and in section 3 we analyze our experimental data using dimensional analysis. In section 4 we apply our results to geological conditions, discuss their implications and the limitations of our work, before concluding in section 5.

## 2. Experimental Method

[11] The behavior of a buoyant dyke in a compressive stress field was investigated by injecting air into a solid of gelatine that was compressed laterally. The solid gelatine was used as an analogue for elastic crustal rocks, and air acted as an analogue for buoyant magma. (Since we are interested in the mechanics and not the dynamics of dyke propagation and sill formation, inviscid air could be used as a magma analogue.) These materials enable us to scale down and investigate at the laboratory scale the elastic and brittle response of magmatic intrusions and elastic rocks to buoyancy and tectonic forces at the geological scale [Menand and Tait, 2002].

[12] The experiments involved varying the amount of injected air, which determined the buoyancy of the crack at the start of its propagation, and the amplitude of the compressive stress applied to the gelatine solid. The experiments were initially carried out in a square-based 40 cm × 40 cm × 30 cm acrylic tank, with equally spaced injection points in its base that allowed several successive experiments to be carried out with a single gelatine solid. Additional experiments were later on carried out with higher buoyancy and lower compressive stress in a taller (30 cm × 30 cm × 50 cm)

acrylic reservoir so that dyke-sill transition could be investigated over larger vertical distances.

### 2.1. Preparation of the Gelatine Solid

[13] High-clarity, 260 bloom, acid, pigskin-derived gelatine in granular form was supplied by Gelita UK Ltd. The gelatine was prepared by dissolving the powder in distilled water. Once complete dissolution of the powder was achieved, the solution was poured into the experimental tank, and left to cool and solidify overnight. To accelerate the solidification process, all experiments were prepared and then performed in a cold room kept at 7°C. A thin layer of oil poured on top of the gelatine solution inhibited water evaporation during the cooling process [Menand and Tait, 2002]. The rigidity of the gelatine was controlled by varying the mass concentration of gelatine (between 2 wt% and 4 wt% in our experiments), and characterized by measuring the gelatine Young's modulus  $E$  following the method of Menand and Tait [2002]. (Knowledge of the gelatine Young's modulus enables also to calculate its fracture toughness  $K_c$  via the relationship  $K_c = \sqrt{2\gamma_s E}$ , where the surface energy of the gelatine  $\gamma_s \simeq 1 \text{ J m}^{-2}$  [Menand and Tait, 2002].)

### 2.2. Lateral Compressive Stress

[14] After solidification, the gelatine solid was in a hydrostatic state of stress (section A1) [see also Takada, 1990]. A lateral deviatoric compressive stress was applied to the gelatine solid by inserting plastic sheets between the solid gelatine and the lateral walls of the tank. These plastic sheets had the same dimensions as the tank walls and covered them entirely to ensure a uniform and homogeneous lateral compressive stress. To facilitate the insertion of these sheets without tearing the gelatine, copper plates were inserted in the tank, against opposite walls, before the gelatine was let to solidify. Once the gelatine was set, hot water was circulated through the copper plates to initiate a slight melting of the gelatine so that it no longer adhered to the copper plates. Plastic sheets could then be easily inserted between the gelatine solid and the copper plates. Several plastic sheets could be successively inserted, thus inducing higher compressive stress.

[15] The insertion of the plastic sheets in the plane  $yOz$  compressed the gelatine solid in the  $x$  direction by an amount equal to the total thickness of the plastic sheets  $u$ . This compression also induced a vertical uplift of the upper free surface of the gelatine solid because the tank walls prevented the gelatine to deform in the  $y$  direction. With a knowledge of the gelatine Young's modulus  $E$  and Poisson's ratio  $\nu$  (0.5 for gelatine [Crisp, 1952; Richards and Mark, 1966]), the compressive stress field generated by the insertion of the plastic sheets can be calculated (see Appendix A)

$$\sigma_x = \frac{4Eu}{3L}, \quad \sigma_y = \frac{2Eu}{3L}, \quad \sigma_z = 0, \quad (1)$$

where  $L$  is the initial lateral extent of the gelatine solid. The compressive stress field is therefore uniform with the maximum compressive stress  $\sigma_1 = \sigma_x$ , the intermediate principal stress  $\sigma_2 = \sigma_y$ , and the least compressive stress  $\sigma_3 = \sigma_z$ ,

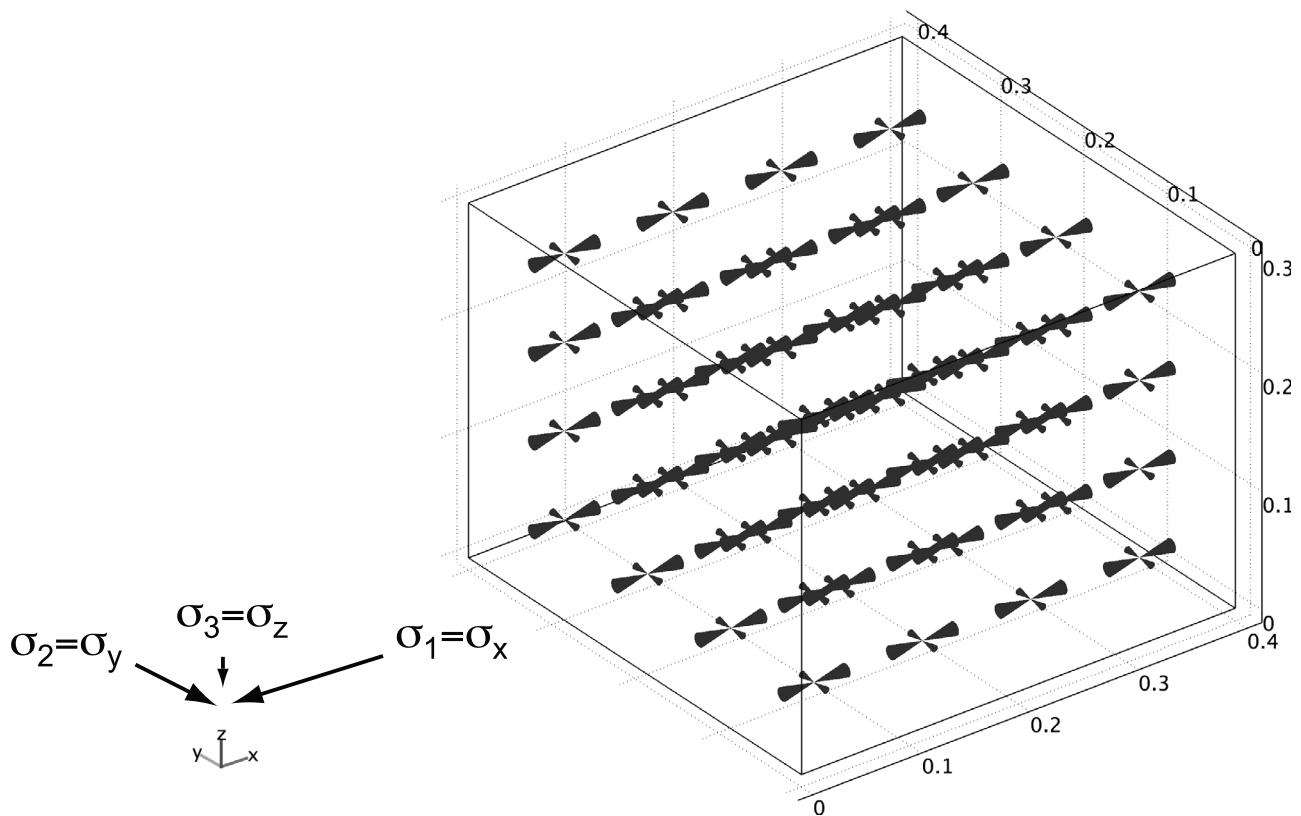


**Figure 1.** Numerical computation of the compressive stress field within the prism of gelatine solid using the finite element software COMSOL Multiphysics (see sections A2 and A3). The compressive stress field appears uniform with principal stresses  $\sigma_1 = \sigma_x = 0.998 \frac{4Eu}{3L}$ ,  $\sigma_2 = \sigma_y = 0.498 \frac{4Eu}{3L}$ , and  $\sigma_3 = \sigma_z = 310^{-11} - 410^{-11}$ . This compressive stress field is independent of the size of the gelatine solid.

which is thus always vertical (Figure 1). Experimental dykes were therefore expected to rotate about a horizontal axis and to ultimately form horizontal sills. The Young's modulus of the gelatine solid was measured just prior to carrying out an experiment following the method of *Menand and Tait* [2002].

### 2.3. Experiments and Data Measurements

[16] For each experiment, once the gelatine solid was set and its Young's modulus measured, a small amount of air was injected with a syringe at the base of the gelatine to initiate a crack parallel to the walls of the tank on which the compression is applied. Air was then withdrawn from that tiny crack, and plastic sheets were inserted to apply the desired compressive stress. The experiment was then carried out by injecting into the pre-existing crack a volume of air, the amount of which was chosen before the start of the experiment. The progression of the air-filled crack was then recorded on video. From the video record (see Movies S1–S3 in auxiliary material), the height of the crack when it started propagating was measured to calculate its buoyancy (referred to as initial height and initial buoyancy, respectively) as well as the vertical distance the crack propagated before turning into a sill in response to the lateral compressive stress. We note that since the applied compressive stress field is

uniform, the effective buoyancy of the crack at the start of each experiment is simply its initial buoyancy.<sup>1</sup>

## 3. Experimental Results

### 3.1. Observations

[17] In all experiments, it was observed that as air was being injected, the crack propagated radially with a penny-shaped geometry in a vertical to sub-vertical plane, including downward movement towards the base of the tank. This condition lasted only a few seconds before the crack stretched out vertically upward. This transition occurred once all of the air had been injected and buoyancy had taken over as the driving force from the pressure induced by injection. From this point, the crack propagated smoothly vertically upward, and with no further influx of air the crack extended and detached from the needle point source, propagating upwards whilst closing fully at its lower tip.

[18] An important observation was that sill did not always form despite the presence of a horizontal compressive stress field. When a small compressive stress was applied, or when a large amount of air was injected into the gelatine solid, the air crack propagated up to the upper free surface of the gelatine with its trajectory barely deviating from the vertical (Movie S1 in auxiliary material).

<sup>1</sup>Auxiliary materials are available in the HTML. doi:10.1029/2009JB006791.

**Table 1.** Experimental Data Associated With Sill Formation<sup>a</sup>

Experiment	$h_0$ (cm)	$d$ (cm)	$E$ (Pa)	$\sigma_x$ (Pa)	$\Pi_1$	$\Pi_2$	Observations
4	4.4	9.4	1713	95.6	$2.1 \pm 0.3$	$4.6 \pm 0.7$	–
6	5.1	12.5	1713	95.6	$2.5 \pm 0.3$	$5.2 \pm 0.7$	–
7	4.1	7.0	4736	268.8	$1.7 \pm 0.2$	$1.5 \pm 0.2$	–
8	5.4	10.0	4736	268.8	$1.8 \pm 0.2$	$2.0 \pm 0.3$	–
12	4.6	15.4	3877	55.6	$3.3 \pm 0.4$	$8.2 \pm 1.2$	–
13	3.7	5.8	3877	389.0	$1.6 \pm 0.3$	$0.9 \pm 0.2$	–
17	2.8	5.3	3734	56.9	$1.9 \pm 0.4$	$4.8 \pm 1.0$	–
18	5.2	7.4	3734	56.9	$1.4 \pm 0.2$	$8.9 \pm 1.5$	–
23	5.5	43.1	3100	29.0	$7.8 \pm 1.5$	$18.7 \pm 3.3$	rotation, wall hit
24	4.1	22.6	3100	29.0	$5.6 \pm 2.0$	$13.7 \pm 2.7$	rotation
34	4.4	42.6	2645	24.6	$9.6 \pm 2.0$	$17.6 \pm 3.3$	rotation, wall hit
35	4.0	35.2	2306	21.6	$8.9 \pm 2.2$	$18.1 \pm 3.6$	rotation, wall hit
36	4.4	43.8	2306	21.6	$10.0 \pm 2.1$	$19.9 \pm 3.8$	rotation, wall hit
44	3.0	50	1564	14.6	$16.9 \pm 3.8$	$19.9 \pm 4.5$	Rotation, surface hit
45	2.7	26.6	1564	14.6	$9.9 \pm 3.3$	$18.2 \pm 4.4$	wall hit

<sup>a</sup> $\Pi_1$  is normalized traveled distance  $d/h_0$ , and  $\Pi_2$  is stress ratio  $(\Delta\rho gh_0)/\sigma_x$ . Observations: rotation indicates rotation around a vertical axis; wall or surface hit occurred before the crack could form a horizontal sill. The uncertainty on the dimensionless ratios  $\Pi_1$  and  $\Pi_2$  takes each observation into account (see text).

[19] Only when a large compressive stress was applied or when the crack had a small volume, did the crack rotate toward the horizontal to form a sill (Movie S2 in auxiliary material). Experiments which lead to sill formation are summarized in Table 1. Sill formation always followed the same pattern. Initially, the crack started to propagate vertically driven by the air buoyancy (Figure 2a). The crack then experienced the horizontal compressive stress that was applied to the gelatine solid, and the crack changed its direction of propagation (Figure 2b). In those experiments where the compressive stress was relatively large, the crack ultimately formed a sill, having turned 90° and stopped its propagation (Figure 2c).

[20] In experiments involving intermediate compressive stress and air amount, the crack deviated and rotated its trajectory towards one of the walls, but the compressive stress was not large enough for a sill to form. Instead the crack was observed to propagate to either the free surface of the gelatine or the wall of the tank at an angle before it could really form a sill (Movie S3 in auxiliary material).

[21] These experimental observations are in accord with the results of previous numerical and analogue studies [e.g., Dahm, 2000; Watanabe et al., 2002], and show that the response of buoyant crack propagating in a horizontal compressive environment is not instantaneous but instead occurs over some distance. If this distance is greater than the vertical extend of the solid the buoyant crack is intruding then the crack will reach the solid surface even though it is in a compressive environment.

### 3.2. Data Analysis

[22] The distance traveled by the crack before it fully formed a sill was found to be determined by a balance between its initial buoyancy, which drove the crack upwards, and the applied horizontal compressive stress that opposed this buoyancy and promoted the formation of the sill: relatively higher buoyancies were observed to favor further propagation distances whereas relatively stronger lateral compressive stress promoted faster crack rotation into sills. In order to quantify this better, experiments were repeated with different amounts of air injected in the gelatine and different compressive stresses applied. In each

experiment, the initial height  $h_0$  of the crack and the vertical distance  $d$  traveled by the crack before its arrest as a sill were measured. Based on our observations, we defined and measured  $h_0$  as the height the crack had when it detached from the needle, which also corresponded to its maximum vertical extension. Experimental data are summarized in Table 1.

[23] Dimensional analysis was used to relate the vertical distance traveled by the crack before it formed a sill to the other parameters. The initial buoyancy of the crack drives it vertically and opposes the effect of the applied horizontal compressive stress. The problem only depends on four parameters characterized by two independent dimensions: the initial height of the crack  $h_0$ , the vertical distance  $d$  traveled by the crack, the initial buoyancy of the crack  $\Delta\rho gh_0$  ( $g$  is the gravitational acceleration, and  $\Delta\rho$  is the density difference between the gelatine and the air), and the applied compressive deviatoric stress  $\sigma_x$ . Dimensional analysis yields the two dimensionless groups

$$\Pi_1 = \frac{d}{h_0}, \quad \Pi_2 = \frac{\Delta\rho gh_0}{\sigma_x}, \quad (2)$$

such that  $\Pi_1 = f(\Pi_2)$  where  $f$  is an unknown function that needs to be determined [Barenblatt, 1996].

[24] When plotting, for all experiments that produced a sill, the final distance traveled by the crack normalized by its initial height  $\Pi_1$  as a function of the stress ratio  $\Pi_2$ , all the experimental data indeed follow a single curve (Figure 3). Careful analysis of the data suggests a linear relationship between  $\ln(\Pi_1)$  and  $\Pi_2$  (Figure 4). Using the method of least squares [Bevington and Robinson, 2003], we find the linear fit

$$\ln(\Pi_1) = (0.36 \pm 0.07) + (0.10 \pm 0.01)\Pi_2, \quad (3)$$

with a correlation coefficient  $R^2 = 0.8964$ . This equation can be re-expressed as the following exponential relationship between the vertical travel distance  $d$  and the other parameters:

$$d = (1.4 \pm 0.1)h_0 \exp\left[(0.10 \pm 0.01)\frac{\Delta\rho gh_0}{\sigma_x}\right]. \quad (4)$$

As expected, when the stress ratio tends to zero (corresponding to negligible initial buoyancy or extremely high remote compressive stress) the crack rotates and turns into a sill over a distance comparable to its initial height. Conversely, when the stress ratio tends to infinity (thus corresponding to negligible remote compressive stress or

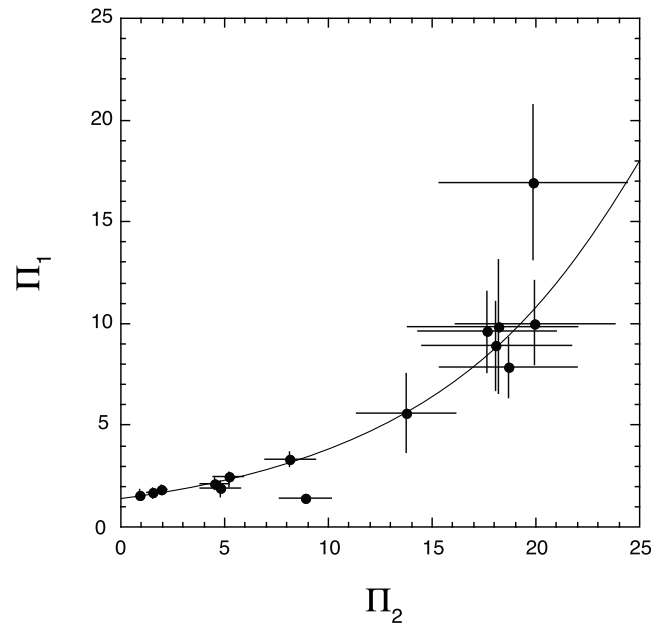
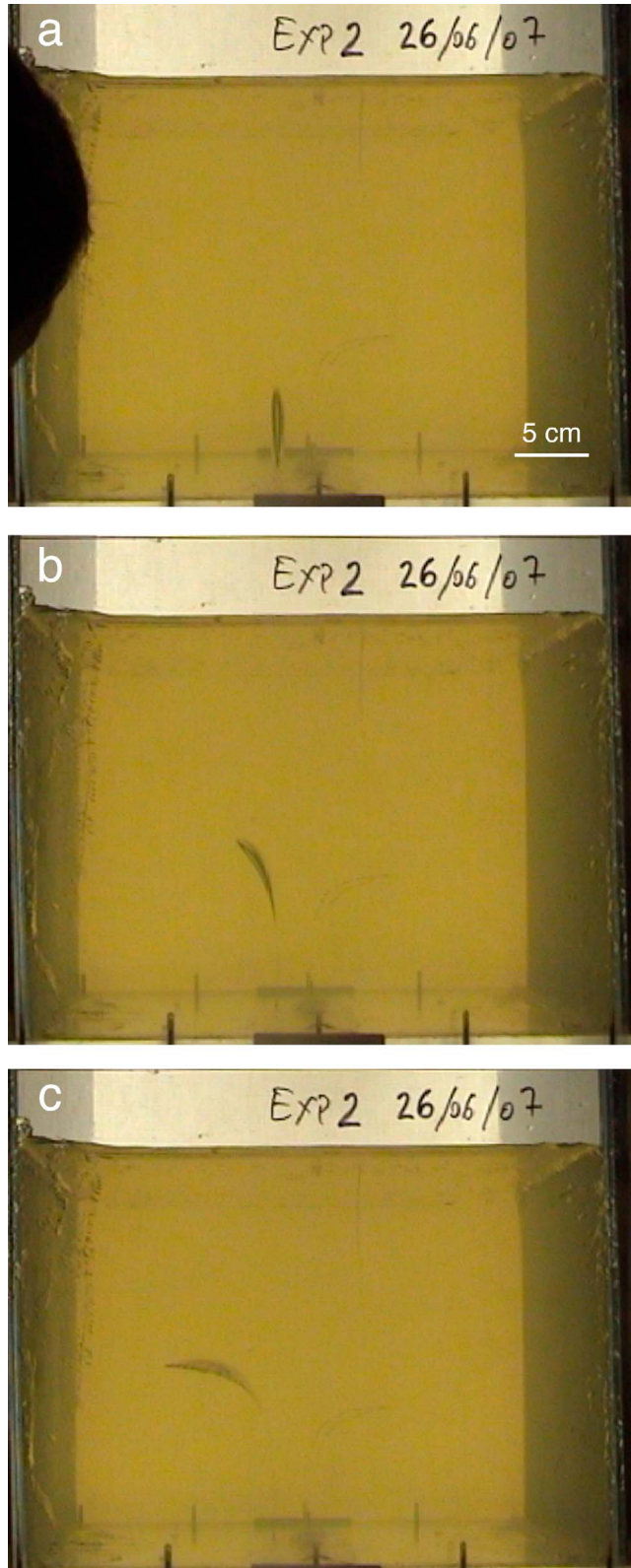


**Figure 3.** Experimental results. The final distance  $d$  traveled by the crack normalized by its initial height  $h_0$  is plotted as a function of the stress ratio  $(\Delta\rho gh_0)/\sigma_x$ . As predicted by dimensional analysis, all data follow a single curve (the solid curve is equation (4)). Each point corresponds to one experiment.

extremely high initial buoyancy) the crack needs to propagate over an infinite distance in order to rotate and form a sill; in effect, sill formation is prevented by the buoyancy of the crack.

### 3.3. Evaluation of the Quality of the Data

[25] Some experimental limitations mean that some of our data have rather large uncertainties. This only affected those experiments carried out in the taller tank (normalized distance  $\Pi_1 > 5$  and stress ratio  $\Pi_2 > 20$ ). We evaluate the possible causes and discuss the implications this would have on the relationship that has just been determined (equation (4)).

[26] As noted previously, in some experiments, the crack propagated towards a tank wall or the free surface of the gelatine before it could form a sill. However, when the crack hit the wall or the surface at a small angle, typically less than  $\sim 30^\circ$  relative to the horizontal, the vertical distance traveled by the crack before it hit the wall or the surface was measured and included to the data set in Table 1. These data, therefore, correspond to under-estimations of the vertical distance the crack would have traveled had the tank been

**Figure 2.** Three successive photographs of an experiment that lead to the formation of a sill. (a) When all the air has been injected into the gelatine solid, the crack stretched vertically and started to detach itself from the needle point source, propagating at a speed of typically a few mm/s. (b) As the crack propagated vertically, driven by the air buoyancy, it felt the applied compressive deviatoric stress and as a consequence started to adjust its trajectory by rotating to the left. (c) Ultimately, the crack rotated to the horizontal and came to a halt as an experimental sill.

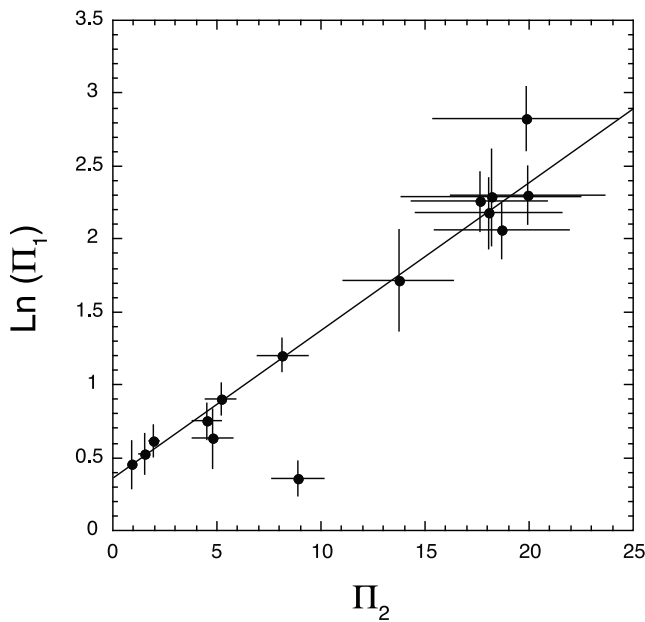


**Figure 4.** Plotting the natural logarithm of the vertical traveled distance as a function of the stress ratio reveals a linear relationship:  $\text{Ln}(\Pi_1) = (0.36 \pm 0.07) + (0.10 \pm 0.01)\Pi_2$  (equation (3)). Correlation coefficient of the fit  $R^2 = 0.8964$ . Each point corresponds to one experiment.

much larger. These under-estimated distances were nevertheless included into the overall data set because they corresponded to some of the highest values of both normalized distance  $\Pi_1$  and stress ratio  $\Pi_2$  of the whole set. From our observations of crack trajectories in experiments where the crack truly stopped and formed a sill, we estimate the under-estimations to be less than 5–10 cm, and these latter values were incorporated into the data uncertainties. We note that our data set is therefore likely to be skewed toward these higher values, but also that data uncertainties, at least partly, take this skewness into account.

[27] Other experiments showed some rotation of the crack around a vertical axis towards or away from the observer. This could reflect the stress field being non-uniform as a result of the gelatine adhering to the tank walls where no deformation was imposed on the gelatine solid (the walls closest and furthest away from the observer). Potentially restricted movement along both these walls would have induced a non-slip boundary condition, which would thus have affected the stress field, causing some rotation of the cracks around a vertical axis. In this case, our stress calculations would therefore overestimate compressive stress and thus skew data towards lower stress ratio  $\Pi_2$ . This potential effect of non-uniform stress field is difficult to quantify, but by comparing the degree of crack rotation around a vertical

axis relative to crack rotation around the horizontal axis  $Oy$  towards plastic sheets, we estimated a maximum additional uncertainty on our stress calculations to be of the order of 10 %.

[28] It is difficult to assess the implication of these potential under-estimations of normalized distance  $\Pi_1$  and over-estimations of stress ratio  $\Pi_2$  on the experimental relationships (3) and (4). We note, however, that the potential increase or decrease in the experimental constants is partly accounted for by the data uncertainties.

## 4. Geological Implications and Limitations

### 4.1. Upscaling to Magmatic Conditions

[29] Dimensional analysis was used to analyze our experimental results, as detailed in section 3. Considering reasonable ranges of natural parameters result in values of the dimensionless ratios falling in the same range as the one investigated in our experiments (Table 2). Thus, our analysis also enables us to upscale our experimental results to magmatic conditions since the experimental constants in equation (4) are dimensionless.

[30] As a dyke propagates away from its source under lithostatic conditions, the effective buoyancy of that dyke increases. *Menand and Tait* [2002] have shown that once the effective buoyancy of the dyke becomes comparable to the source overpressure, it becomes the main driving force and the dyke then propagates steadily. The height of the buoyant dyke at that point, which we defined as its initial height  $h_0$  in our experiments, is not really well constrained but can be estimated, however, from the dyke overpressure, which depends on the initial stress conditions in the source region.

[31] Here, we assume that a buoyant dyke rises from a source under lithostatic conditions and then, some distance from the source, enters a region of the crust subjected to a horizontal compressive deviatoric stress. We assume that initially, as the dyke leaves its source, buoyancy is negligible and that the magma overpressure,  $\Delta P$ , in the source drives the dyke away from the source region.

[32] It can be constrained by the tensile strength of surrounding rocks,  $T_s$ , so that

$$\Delta P \simeq T_s. \quad (5)$$

The effective buoyancy becomes the main driving force of the dyke when it becomes comparable to the source overpressure so that

$$\Delta P = \Delta \rho g h_0. \quad (6)$$

At this point, the buoyant dyke has reached its initial buoyant height  $h_0$  and subsequently propagates in a steady-state

**Table 2.** Parameters and Dimensionless Ratios in Nature and Experiments<sup>a</sup>

	$h_0$ (m)	$d$ (m)	$\Delta \rho$ (kg/m <sup>3</sup> )	$\sigma_x$ (Pa)	$T_s$ (Pa)	$\Pi_1$	$\Pi_2$
Experiment	0.02–0.06	0.05–0.5	1000	15–390	–	1–17	1–20
Nature	200–10 <sup>4</sup>	100–10 <sup>4</sup>	100–500	10 <sup>5</sup> –10 <sup>8</sup>	10 <sup>6</sup> –10 <sup>7</sup>	0.01–50	0.01–100

<sup>a</sup>The experimental value for  $\Delta \rho$  neglects the density of air and thus corresponds to that of gelatine [*Di Giuseppe et al.*, 2009]. Other experimental values are taken from Table 1. Natural values for  $h_0$  are estimated from equation (7). Other ranges of natural values are taken as representative of geological conditions.

[Menand and Tait, 2002] until it enters a region of the crust that is subject to some deviatoric stress field. These two different expressions for magma overpressure can be combined to express the initial height of the dyke as a function of the rock tensile strength and the density difference between magma and rocks

$$h_0 \simeq \frac{T_s}{\Delta\rho g}. \quad (7)$$

[33] Alternatively, we can define the magma overpressure needed to initiate dyke propagation as that for which the resistance to fracture, or fracture toughness  $K_c$ , of the source rocks is exceeded (which depends on the dyke height  $h$ , and thus corresponds to a length-scale dependent tensile strength)

$$\Delta P \simeq \frac{K_c}{\sqrt{h}}, \quad (8)$$

in which case the dyke becomes buoyancy-driven when its initial height

$$h_0 \simeq \left(\frac{K_c}{\Delta\rho g}\right)^{2/3}. \quad (9)$$

[34] We assume that the dyke propagates some distance and becomes fully driven by buoyancy before entering a region where a compressive deviatoric stress acts horizontally. For the sake of simplicity, we also assume that this deviatoric stress is uniform with value  $\sigma_x$ . Combining equation (7) with our experimental expression (4) gives the vertical distance the buoyant dyke would have to propagate within the region under compression before turning into a sill in response to the deviatoric stress  $a_x$

$$d \simeq \frac{T_s}{\Delta\rho g} \exp\left[(0.10 \pm 0.01) \left(\frac{T_s}{\sigma_x}\right)\right]. \quad (10)$$

Using equation (9) instead yields

$$d \simeq \left(\frac{K_c}{\Delta\rho g}\right)^{2/3} \exp\left[(0.10 \pm 0.01) \frac{(\Delta\rho g K_c^2)^{1/3}}{\sigma_x}\right]. \quad (11)$$

[35] Equations (10) and (11) are represented in Figure 5 as a function of the compressive stress for a range of density differences, 100–500 kg/m<sup>3</sup>, two different tensile strengths, 1 and 10 MPa, and a corresponding range of fracture toughness 10–1000 Pa m<sup>1/2</sup> (see equations (7) and (9)). Figure 5 shows that the dyke-to-sill transition takes place over some non-negligible distance. Over the range of geological parameters considered here, Figure 5 shows that a dyke propagating in homogeneous, elastic rocks would require a minimum distance of two hundred meters, and in most cases of the order of one to ten kilometers, to fully adjust to a horizontal compressive stress field and turn into a sill.

[36] As expected, Figure 5 shows that dykes entering regions that are subjected to higher compressive deviatoric stresses would adjust more rapidly to those stresses and

thus form sills over shorter vertical distances. However, even for very high compressive stress, the dyke-to-sill transition does not happen instantaneously but instead occurs over a minimum distance of the order of the initial buoyant height of the dyke (see equation (4)).

[37] Figure 5 also shows that a dyke propagating through stiffer rocks would need to propagate over a greater distance before forming a sill. This can be understood by recalling that a dyke originating from a stiffer rock region would need a higher source overpressure in order to overcome that relatively higher rock resistance to fracture which in turn would result in a higher subsequent driving effective buoyancy. This higher effective buoyancy would then be able to drive the dyke over a greater distance before it fully rotates into a sill.

#### 4.2. Implications for the Formation of Sills

[38] Equations (10) and (11) represent the distance over which a buoyant dyke would transform into a sill owing to remote compressive deviatoric stress in homogeneous elastic rocks. In the absence of crustal heterogeneities, a stress-controlled dyke-to-sill transition would occur over a minimum distance of two hundred meters, and presumably of several kilometers in most cases (Figure 5).

[39] This contrasts with the fact that the crust involves a large number of strata with different mechanical properties that alternate rapidly. For instance, the Michigan basin sedimentary strata exhibit vertical density variations over distances ranging from few tens to several hundred of meters [Hinze *et al.*, 1978]. Likewise, composite volcanoes and rift zones in Iceland are composed of layers with contrasting mechanical properties, mostly pyroclastic rocks, lava flows and other igneous sheets, many of which are only a few meters thick although some unit thicknesses can reach up to 100 m [Gudmundsson, 2003; Gudmundsson and Phillip, 2006].

[40] Our study shows that the characteristic length-scale for stress-controlled sill formation is typically greater (and in many instances much greater) than the average thickness of lithological units. In accord with previous studies [e.g., Dahm, 2000; Watanabe *et al.*, 2002], our experiments show also that dykes would reach the surface even in a compressive tectonic environment if the characteristic length-scale for a dyke-to-sill transition is greater than the distance that separates them from the surface. This contrasts with the field observations that only a few percentage of dykes reach the surface, and that not all the dykes that do not reach the surface turns into sills [Gudmundsson *et al.*, 1999].

[41] These findings reinforces the point made by previous studies that crustal heterogeneities play an important role in determining where in the crust sills form, even when dykes are subject to horizontal compressive deviatoric stress. Contrasts in mechanical and rheological properties can indeed arrest the advance of dykes and lead to sill emplacement [Mudge, 1968; Gudmundsson and Brenner, 2001; Gudmundsson, 2003; Kavanagh *et al.*, 2006; Taisne and Jaupart, 2009]. Moreover, the finding that stress-controlled sill formation operates over distances that likely encompass numerous crustal strata would also imply that a stress control on sill formation involves almost certainly some stress interactions with these rock strata [Gretener, 1969; Gudmundsson, 1986; Gudmundsson and Phillip,

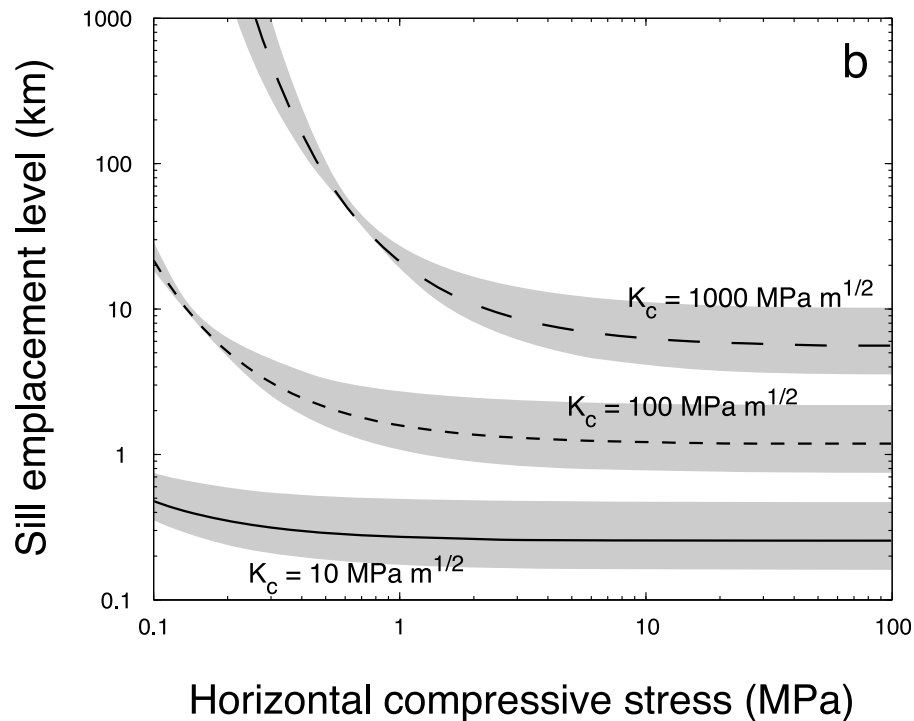
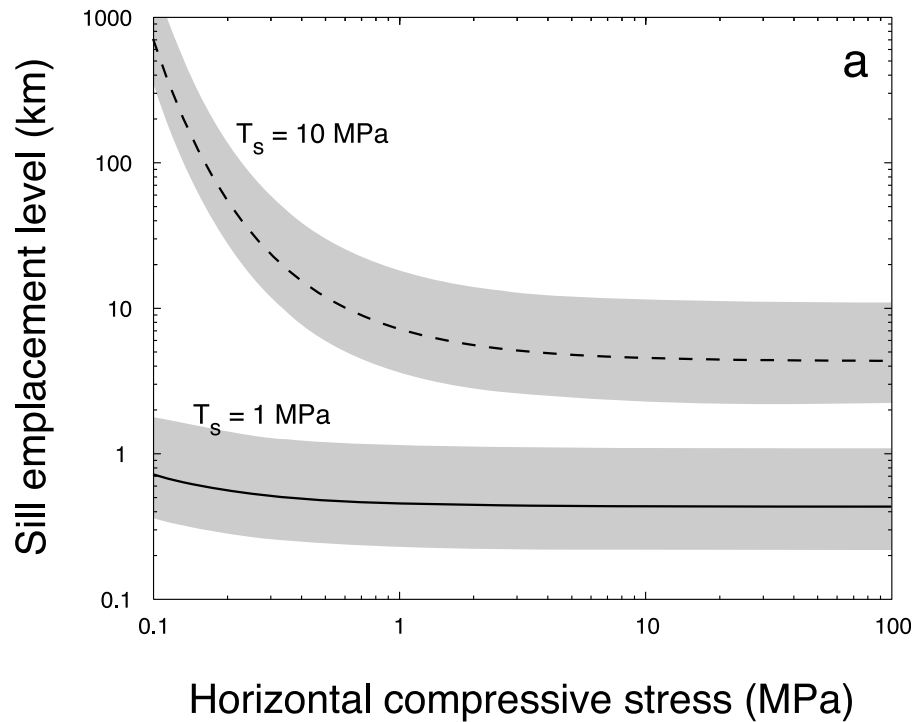


**Figure 5.** Upscaling to magmatic conditions: the vertical distance a dyke has to propagate before turning into a sill is represented as a function of the ambient horizontal compressive stress (equations (10) and (11)). (a) The two curves correspond to two different rock tensile strengths,  $T_s = 1$  MPa (solid curve) and  $T_s = 10$  MPa (dashed curve), and the grey areas represent a range of density differences between 100 and 500  $\text{kg/m}^3$ . (b) The three curves correspond to three different fracture toughnesses,  $K_c = 10$   $\text{MPa m}^{1/2}$  (solid curve),  $K_c = 100$   $\text{MPa m}^{1/2}$  (short-dashed curve) and  $K_c = 1000$   $\text{MPa m}^{1/2}$  (long-dashed curve), and the grey areas represent a range of density differences between 100 and 500  $\text{kg/m}^3$ .

2006]. These stress interactions must therefore be taken into account when considering potential stress control on the emplacement of sills and indeed on the mechanical behavior of igneous sheets.

#### 4.3. Limitation of Our Analysis

[42] Our experiments and analysis have only considered the case of buoyancy-driven cracks, when dykes could also be driven by their source overpressure. Indeed, a dyke overpressure is really the sum of that from its source and of the dyke effective buoyancy, minus the loss due to viscous pressure drop.

[43] Once the effective buoyancy is large enough and becomes comparable to the source overpressure, it becomes the main driving force of a steady-state propagation [Menand and Tait, 2002]. We note, however, that as a buoyant dyke modifies its trajectory in response to a horizontal compressive stress, it would also experience a decrease in effective buoyancy owing to a reduction in its vertical extent. Indeed, propagation of buoyant dykes is controlled by the local effective buoyancy balance that takes place at the dyke nose region [Lister and Kerr, 1991]. In our experiments, the air-filled cracks represent the dyke nose region. (The elastic gelatine solid closes shut behind these cracks because of the inviscid air, whereas if the cracks were filled by a viscous fluid, as magma-filled dykes are, then the dykes would develop a tail behind their nose region. Yet, in this latter case the material left within the tail would not contribute to the force budget that drives crack propagation; buoyancy crack propagation is entirely and only controlled by local effective buoyancy considerations [Lister and Kerr, 1991].) Therefore, as a buoyant dyke starts adjusting its trajectory to a horizontal compressive stress field and starts turning into a sill, the vertical extent over which the effective buoyancy balance operates decreases. Ultimately this vertical dimension is the thickness of the new sill formed by the complete rotation of the dyke.

[44] The case we have not dealt with is that of dykes entering compressive regions before they are fully driven by buoyancy. In this case, source overpressure and potential viscous pressure drop should be taken into account. If one assumes that a dyke overpressure remains essentially constant then, by definition, this dyke would continually experience the same constant internal driving pressure, and thus would be expected, perhaps paradoxically, to be able to rise vertically further than a buoyancy-driven dyke (which would instead experience a continuous reduction in effective buoyancy). One would therefore expect, everything else being equal, constant-pressure-driven dykes to adjust their course to a horizontal compressive stress over greater vertical distances when compared to buoyant dykes.

[45] However, dyke overpressure is likely not to remain constant because magma withdrawal from the source into the dyke and viscous pressure drop would continuously reduce it whilst the effective buoyancy would continuously increase it (before the dyke enters the compressive region). The response of such a vertically-propagating pressure-driven dyke to horizontal compressive stress cannot be deduced from our buoyant experiments, and would require addressing the dynamics of such a pressure-driven dyke. Nevertheless, what our work suggests, in conjunction with the observation that most dykes get arrested by crustal

heterogeneities, is that these heterogeneities are likely to be very important in affecting the trajectories of dykes and in controlling where sills form.

## 5. Conclusions

[46] Using analogue experiments, the behavior of a buoyant crack rising through a horizontal compressive deviatoric stress field in a homogeneous elastic solid has been investigated and quantified. These experiments show that the horizontal compressive stress opposes the vertical advance of the buoyant crack, and forces the crack to modify its trajectory into the horizontal plane.

[47] The experimental data show how the balance between the driving effective buoyancy and the deviatoric horizontal compressive stress determines the vertical distance over which the crack rotation takes place. Using dimensional analysis, the characteristic length-scale for this dyke-to-sill rotation is shown to increase exponentially with the ratio of the initial crack effective buoyancy to horizontal compressive stress. If this length-scale is larger than the distance that separates the crack from the surface then the crack reaches the surface even though it is subject to a horizontal compressive deviatoric stress. Conversely, if this length-scale is smaller then the crack stops its propagation as a sill despite being buoyant.

[48] When upscaled to magmatic conditions and over a range of typical values for tensile strength, fracture toughness, density difference and deviatoric compressive stress, our results suggest that a dyke propagating through homogeneous elastic rocks would need to propagate vertically over a minimum distance of two hundred meters and more likely of several kilometers in most cases before it could form a sill in response to the horizontal compressive deviatoric stress.

[49] The characteristic length-scale for stress-controlled sill formation is typically greater than the average thickness of lithological units, which thus supports the idea that crustal heterogeneities play an important role in determining the fate of dykes and in controlling where sills form, and that a stress control on igneous sheets propagation and sill formation most likely involves stress interactions with and redistribution within rock strata.

## Appendix A: State of Stress of the Gelatin Solid

[50] Stresses  $\sigma$  and strains  $\epsilon$  in an elastic solid can be linearly related according to Hooke's law, which in Cartesian coordinates is expressed as

$$\begin{aligned}\epsilon_x &= \frac{1}{E} [\sigma_x - \nu(\sigma_y + \sigma_z)], \\ \epsilon_y &= \frac{1}{E} [\sigma_y - \nu(\sigma_x + \sigma_z)], \\ \epsilon_z &= \frac{1}{E} [\sigma_z - \nu(\sigma_x + \sigma_y)],\end{aligned}\tag{A1}$$

where  $E$  and  $\nu$  are the Young's modulus and Poisson's ratio of the elastic solid, respectively [Timoshenko and Goodier, 1970].

### A1. Initial State of Stress

[51] Initially, the gelatine solid adheres to the tank walls and so there is no horizontal strain,  $\epsilon_x = \epsilon_y = 0$ . Using Hooke's law (A1), we obtain the following relationship between the three stress components:

$$\sigma_x = \sigma_y = \frac{\nu}{(1-\nu)}\sigma_z. \quad (\text{A2})$$

Given that gelatine has a Poisson's ratio  $\nu = 0.5$  [Crisp, 1952; Richards and Mark, 1966],  $\sigma_x = \sigma_y = \sigma_z$  and the initial stress field is hydrostatic.

### A2. Compressive Stress Field

[52] Gelatine is compressed by imposing a horizontal displacement  $u$  in the  $x$  direction, whilst the tank walls prevent any deformation in the horizontal  $y$  direction. This induces a horizontal deformation  $\epsilon_x = \frac{u}{L}$  ( $L$  is the initial lateral extent of the gelatine solid) and  $\epsilon_y = 0$ . This reduces Hooke's law (A1) to

$$\begin{aligned} E\epsilon_x &= \sigma_x - \nu\sigma_y - \nu\sigma_z, \\ \sigma_y &= \nu\sigma_x + \nu\sigma_z, \end{aligned} \quad (\text{A3})$$

$$E\epsilon_z = \sigma_z - \nu\sigma_x - \nu\sigma_y,$$

from which we obtain

$$E\epsilon_x = \frac{(1+\nu)(1-2\nu)}{(1-\nu)}\sigma_x - \frac{\nu}{(1-\nu)}E\epsilon_z. \quad (\text{A4})$$

Gelatine Poisson's ratio  $\nu = 0.5$ , and it follows that

$$\epsilon_x = -\epsilon_z. \quad (\text{A5})$$

Combining this expression with the modified Hooke's law (A3) for a Poisson's ratio of 0.5, we obtain

$$\sigma_x = \frac{4}{3}E\epsilon_x + \sigma_z, \quad \sigma_y = \frac{2}{3}E\epsilon_x + \sigma_z. \quad (\text{A6})$$

The vertical stress  $\sigma_z$  cannot be calculated analytically because the modified Hooke's law (A3) reduces to a system of two equations with three unknowns in the limit of a Poisson's ratio  $\nu = 0.5$ . Finite element computations were therefore carried out to evaluate  $\sigma_z$  (section A3). These numerical calculations indicate that the vertical stress is nil, and therefore, recalling that  $\epsilon_x = \frac{u}{L}$ , that the compressive stress field within the prism of solid gelatine is

$$\sigma_x = \frac{4Eu}{3L}, \quad \sigma_y = \frac{2Eu}{3L}, \quad \sigma_z = 0. \quad (\text{A7})$$

The compressive stress field is thus uniform with  $\sigma_x$  as the maximum compressive stress,  $\sigma_y$  the intermediate principal stress, and  $\sigma_z$  the least compressive stress which is thus always vertical.

### A3. Numerical Validation

[53] The finite element software COMSOL Multiphysics was used to evaluate the three-dimensional stress field within the elastic gelatin solid, and to test the validity of the expressions for the compressive stresses (A6). The geometry

was that of the gelatine prism, and the boundary conditions were identical to those in the experiments: imposed displacement  $u$  in the  $x$  direction, no displacement in the  $y$  direction, no displacement at the base of the prism and a free upper surface. A displacement  $u = 8$  mm and a Young's modulus  $E = 2000$  Pa were chosen as representative of the experimental values, whereas the Poisson's ratio  $\nu$  had value 0.499 since a value of 0.5 could not be handled numerically.

[54] Figure 1 shows that the compressive stress field is uniform, with the maximum compressive stress being  $\sigma_x$  and the least compressive stress being  $\sigma_z$ . To test the validity of the analytical expressions of the compressive stresses (A6), the computed principal stress values have been normalized by  $\sigma_x$  theoretical value  $\frac{4Eu}{3L}$ . Computed normalized values gives  $\sigma_x = 0.998$ ,  $\sigma_y = 0.498$ , and  $\sigma_z$  in the range  $310^{-11}$ – $410^{-11}$ .

[55] **Acknowledgments.** Agust Gudmundsson and Olivier Merle are thanked for their constructive comments on an earlier version of the manuscript. We also thank the Associate Editor and three anonymous reviewers for their constructive reviews and comments which lead to substantial improvement of the manuscript. This research was supported by a Leverhulme Trust research grant.

### References

- Annen, C., and R. S. J. Sparks (2002), Effects of repetitive emplacement of basaltic intrusions on thermal evolution and melt generation in the crust, *Earth Planet. Sci. Lett.*, *203*, 937–955.
- Annen, C., J. D. Blundy, and R. S. J. Sparks (2006), The sources of granitic melt in deep hot zones, *Trans. R. Soc. Edinburgh Earth Sci.*, *97*, 297–309.
- Antonellini, M. A., and F. W. Cambray (1992), Relations between sill intrusions and bedding-parallel extensional shear zones in the Mid-continent Rift System of the Lake Superior region, *Tectonophysics*, *202*, 331–349.
- Barenblatt, G. I. (1996), *Scaling, Self-Similarity, and Intermediate Asymptotics*, Cambridge Univ. Press, Cambridge, U. K.
- Bedard, J. H., R. S. J. Sparks, M. Renner, M. J. Cheadle, and M. A. Hallworth (1988), Peridotite sills and metasomatic gabbros in the Eastern Layered Series of the Rhum complex, *J. Geol.*, *145*, 207–224.
- Belcher, R. W., and A. F. M. Kisters (2006), Progressive adjustments of ascent and emplacement controls during incremental construction of the 3.1 Ga Heerenveen batholith, South Africa, *J. Struct. Geol.*, *28*, 1406–1421.
- Bevington, P. R., and D. K. Robinson (2003), *Data Reduction and Error Analysis for the Physical Sciences*, McGraw-Hill, Boston.
- Burchardt, S. (2008), New insights into the mechanics of sill emplacement provided by field observations of the Njardvik Sill, northeast Iceland, *J. Volcanol. Geotherm. Res.*, *173*, 280–288.
- Cartwright, J., and D. M. Hansen (2006), Magma transport through the crust via interconnected sill complexes, *Geology*, *34*, 929–932.
- Coleman, D. S., W. Gray, and A. F. Glazner (2004), Rethinking the emplacement and evolution of zoned plutons: Geochronologic evidence for incremental assembly of the Tuolumne Intrusive Suite, California, *Geology*, *32*, 433–436.
- Corry, C. E. (1988), *Laccoliths: Mechanics of Emplacement and Growth*, *Geol. Soc. Am. Spec. Pap. Ser.*, vol. 220, Geol. Soc. of Am., Boulder, Colo.
- Crisp, J. A. (1984), Rates of magma emplacements and volcanic output, *J. Volcanol. Geotherm. Res.*, *20*, 177–211.
- Crisp, J. D. C. (1952), The use of gelatin models in structural analysis, *Proc. Inst. Mech. Eng. Part B*, *1B(12)*, 580–604.
- Dahm, T. (2000), Numerical simulations of the propagation path and the arrest of fluid-filled fractures in the Earth, *Geophys. J. Int.*, *141*, 623–638.
- de Saint-Blanquat, M., G. Habert, E. Horsman, S. S. Morgan, B. Tikoff, P. Launeau, and G. Gleizes (2006), Mechanisms and duration of non-tectonically assisted magma emplacement in the upper crust: The Black Mesa pluton, Henry Mountains, Utah, *Tectonophysics*, *48*, 1–31.
- Di Giuseppe, E., F. Funicello, F. Corbi, G. Ranalli, and G. Mojoli (2009), Gelatins as rock analogs: A systematic study of their rheological and physical properties, *Tectonophysics*, *473*, 391–403.
- Fridleifsson, I. B. (1977), Distribution of large basaltic intrusions in the Icelandic crust and the nature of the layer 2–layer 3 boundary, *Geol. Soc. Am. Bull.*, *88*, 1689–1693.

- Gilbert, G. K. (1877), Geology of the Henry Mountains, Utah, in *U.S. Geographical and Geological Survey of the Rocky Mountain Region*, report, pp. 1–160, Gov. Print. Off., Washington, D. C.
- Glazner, A. F., J. M. Bartley, D. S. Coleman, W. Gray, and R. Z. Taylor (2004), Are plutons assembled over millions of years by amalgamation from small magma chambers?, *GSA Today*, *14*, 4–11.
- Greener, P. E. (1969), On the mechanics of the intrusion of sills, *Can. J. Earth Sci.*, *6*, 1415–1419.
- Gudmundsson, A. (1986), Formation of crustal magma chambers in Iceland, *Geology*, *14*, 164–166.
- Gudmundsson, A. (1990), Emplacement of dikes, sills and crustal magma chambers at divergent plate boundaries, *Tectonophysics*, *176*, 257–275.
- Gudmundsson, A. (2003), Surface stresses associated with arrested dykes in rift zones, *Bull. Volcanol.*, *65*, 606–619.
- Gudmundsson, A., and S. L. Brenner (2001), How hydrofractures become arrested, *Terra Nova*, *13*, 456–462.
- Gudmundsson, A., and S. L. Phillip (2006), How local stress fields prevent volcanic eruptions, *J. Volcanol. Geotherm. Res.*, *158*, 257–268.
- Gudmundsson, A., L. B. Marinoni, and J. Marti (1999), Injection and arrest of dykes: Implications for volcanic hazards, *J. Volcanol. Geotherm. Res.*, *88*, 1–13.
- Hinze, W. J., J. W. Bradley, and A. R. Brown (1978), Gravimeter survey in the Michigan Basin deep borehole, *J. Geophys. Res.*, *83*, 5864–5868.
- Holness, M. B., and M. C. S. Humphreys (2003), The Traigh Bhàn na Sgùrra sill, Isle of Mull: Flow localization in a major magma conduit, *J. Petrol.*, *44*, 1961–1976.
- Horsman, E., B. Tikoff, and S. Morgan (2005), Emplacement-related fabric and multiple sheets in the Maiden Creek sill, Henry Mountains, Utah, USA, *J. Struct. Geol.*, *27*, 1426–1444.
- Horsman, E., S. Morgan, M. de Saint-Blanquat, G. Habert, R. Hunter, A. Nugent, and B. Tikoff (2008), Emplacement and assembly of shallow intrusions from multiple magma pulses, Henry Mountains, Utah, in *Sixth Hutton Symposium on the Origin of Granite and Related Rocks*, edited by A. F. E. A. Kisters, R. Soc. of Edinburgh, Edinburgh, in press.
- Hutton, D. H. W. (1992), Granite sheeted complexes: Evidence for the dyking ascent mechanism, *Trans. R. Soc. Edinburgh Earth Sci.*, *83*, 377–382.
- Hyndman, D. W., and D. Alt (1987), Radial dikes, laccoliths and gelatin models, *J. Geol.*, *95*, 763–774.
- John, B. E. (1988), Structural reconstruction and zonation of a tilted mid-crustal magma chamber: The felsic Chemehuevi Mountains plutonic suite, *Geology*, *16*, 613–617.
- John, B. E., and J. D. Blundy (1993), Emplacement-related deformation of granitoid magmas, southern Adamello Massif, Italy, *Geol. Soc. Am. Bull.*, *105*, 1517–1541.
- Johnson, A. M., and D. D. Pollard (1973), Mechanics of growth of some laccolithic intrusions in the Henry Mountains, Utah, part I. Field observations, Gilbert's model, physical properties and flow of the magma, *Tectonophysics*, *18*, 261–309.
- Kavanagh, J. L., T. Menand, and R. S. J. Sparks (2006), An experimental investigation of sill formation and propagation in layered elastic media, *Earth Planet. Sci. Lett.*, *245*, 799–813.
- Kühn, D., and T. Dahm (2004), Simulation of magma ascent by dykes in the mantle beneath mid-ocean ridges, *J. Geodyn.*, *38*, 147–159.
- Kühn, D., and T. Dahm (2008), Numerical modelling of dyke interaction and its influence on oceanic crust formation, *Tectonophysics*, *447*, 53–65.
- Lister, J. R., and R. C. Kerr (1991), Fluid-mechanical models of crack propagation and their application to magma transport in dykes, *J. Geophys. Res.*, *96*, 10,049–10,077.
- Menand, T. (2008), The mechanics and dynamics of sills in elastic layered media and their implications for the growth of laccoliths, *Earth Planet. Sci. Lett.*, *267*, 93–99.
- Menand, T., and S. R. Tait (2002), The propagation of a buoyant liquid-filled fissure from a source under constant pressure: An experimental approach, *J. Geophys. Res.*, *107*(B11), 2306, doi:10.1029/2001JB000589.
- Mériaux, C., and J. R. Lister (2002), Calculation of dike trajectories from volcanic centers, *J. Geophys. Res.*, *107*(B4), 2077, doi:10.1029/2001JB000436.
- Michaut, C., and C. Jaupart (2006), Ultra-rapid formation of large volumes of evolved magma, *Earth Planet. Sci. Lett.*, *250*, 38–52.
- Morgan, S. S., E. Horsman, B. Tikoff, M. de Saint-Blanquat, and G. Habert (2005), Sheet-like emplacement of satellite laccoliths, sills and bysmaliths of the Henry Mountains, southern Utah, in *Interior Western United States, Geol. Soc. Am. Field Guide Ser.*, vol. 6, edited by J. Pederson and C. M. Dehler, pp. 283–309, doi:10.1130/2005.fld006(14), Geol. Soc. of Am., Boulder, Colo.
- Morgan, S. S., A. Stanik, E. Horsman, B. Tikoff, M. de Saint-Blanquat, and G. Habert (2008), Emplacement of multiple magma sheets and wall rock deformation: Trachyte Mesa intrusion, Henry Mountains, Utah, *J. Struct. Geol.*, *30*, 491–512.
- Mudge, M. R. (1968), Depth control of some concordant intrusions, *Geol. Soc. Am. Bull.*, *79*, 315–332.
- Muller, O. H., and D. D. Pollard (1977), The stress state near Spanish Peaks, Colorado determined from a dike pattern, *Pure Appl. Geophys.*, *115*, 69–86.
- Odé, H. (1957), Mechanical analysis of the dike pattern of the Spanish Peaks area, Colorado, *Geol. Soc. Am. Bull.*, *68*, 567–576.
- Parsons, T., N. H. Sleep, and G. A. Thompson (1992), Host rock rheology controls on the emplacement of tabular intrusions: Implications for underplating of extending crust, *Tectonics*, *11*, 1348–1356.
- Pasquaré, F., and A. Tibaldi (2007), Structure of a sheet-laccolith system revealing the interplay between tectonic and magma stresses at Stardalur Volcano, Iceland, *J. Volcanol. Geotherm. Res.*, *161*, 131–150.
- Pinel, V., and C. Jaupart (2000), The effect of edifice load on magma ascent beneath a volcano, *Philos. Trans. R. Soc. London A*, *358*, 1515–1532.
- Pinel, V., and C. Jaupart (2004), Magma storage and horizontal dyke injection beneath a volcanic edifice, *Earth Planet. Sci. Lett.*, *221*, 245–262.
- Richards, R., Jr., and R. Mark (1966), Gelatin models for photoelastic analysis of gravity structures, *Exp. Mech.*, *6*, 30–38.
- Rivalta, E., and T. Dahm (2006), Acceleration of buoyancy-driven fractures and magmatic dikes beneath the free surface, *Geophys. J. Int.*, *166*, 1424–1439.
- Rivalta, E., M. Böttlinger, and T. Dahm (2005), Buoyancy-driven fracture ascent: Experiments in layered gelatine, *J. Volcanol. Geotherm. Res.*, *144*, 273–285.
- Roman, D. C., S. C. Moran, J. A. Power, and K. V. Cashman (2004), Temporal and spatial variation of local stress fields before and after the 1992 eruptions of Crater Peak Vent, Mount Spurr volcano, Alaska, *Bull. Seismol. Soc. Am.*, *94*, 2366–2379.
- Roman, D. C., J. Neuberg, and R. R. Luckett (2006), Assessing the likelihood of volcanic eruption through analysis of volcanotectonic earthquake fault plane solutions, *Earth Planet. Sci. Lett.*, *248*, 244–252.
- Shaw, H. R. (1985), Links between magma-tectonic plate balances, plutonism, and volcanism, *J. Geophys. Res.*, *90*, 11,275–11,288.
- Takada, A. (1989), Magma transport and reservoir formation by a system of propagating cracks, *Bull. Volcanol.*, *52*, 118–126.
- Taisne, B., and C. Jaupart (2009), Dike propagation through layered rocks, *J. Geophys. Res.*, *114*, B09203, doi:10.1029/2008JB006228.
- Takada, A. (1990), Experimental study on propagation of liquid-filled crack in gelatin: Shape and velocity in hydrostatic stress condition, *J. Geophys. Res.*, *95*, 8471–8481.
- Thomson, K. (2007), Determining magma flow in sills, dykes and laccoliths and their implications for sill emplacement mechanisms, *Bull. Volcanol.*, *70*, 183–201.
- Timoshenko, S. P., and J. N. Goodier (1970), *Theory of Elasticity*, 3rd ed., McGraw-Hill, Singapore.
- Vigneress, J. L., and J. L. Bouchez (1997), Successive granitic magma batches during pluton emplacement: The case of Cabeza de Araya (Spain), *J. Petrol.*, *38*, 1767–1776.
- Watanabe, T., T. Koyaguchi, and T. Seno (1999), Tectonic stress controls on ascent and emplacement of magmas, *J. Volcanol. Geotherm. Res.*, *91*, 65–78.
- Watanabe, T., T. Masuyama, K. Nagaoka, and T. Tahara (2002), Analog experiments on magma-filled cracks: Competition between external stresses and internal pressure, *Earth Planets Space*, *54*, 1247–1261.
- Westergaard, H. M. (1939), Bearing pressures and cracks, *Trans. Am. Soc. Mech. Eng.*, *61*, A49–A53.
- Wiebe, R. A., and W. J. Collins (1998), Depositional features and stratigraphic sections in granitic plutons: Implications for the emplacement and crystallization of granitic magma, *J. Struct. Geol.*, *20*, 1273–1289.

P. Bengehiat, Atlas Iron Limited, PO Box 223, West Perth, WA 6872, Australia. (philipb@atlasiron.com.au)

K. A. Daniels and T. Menand, Centre for Environmental and Geophysical Flows, Department of Earth Sciences, University of Bristol, Wills Memorial Building, Queen's Road, Bristol BS8 1RJ, UK. (k.a.daniels@bristol.ac.uk; t.menand@bristol.ac.uk)